

The Effects of Machine Components on Bifurcation and Chaos as Applied to Multimachine System

Majdi M. Alomari and Benedykt S. Rodanski
University of Technology, Sydney (UTS)
P.O. Box 123, Broadway NSW 2007, Australia
(e-mail: majdi.m.alomari@eng.uts.edu.au)

Abstract: The second system of the IEEE second benchmark model of Subsynchronous Resonance (SSR) is considered. The system can be mathematically modeled as a set of first order nonlinear ordinary differential equations with the compensation factor ($\mu = X_c/X_t$) as a bifurcation (control) parameter. So, bifurcation theory can be applied to nonlinear dynamical systems, which can be written as $dx/dt=F(x;\mu)$. The effects of machine components, i.e. damper winding, automatic voltage regulator (AVR), and power system stabilizer (PSS) on SSR in power system are studied. The results show that these components affect the locations, number and type of the Hopf bifurcations.

Keywords: Hopf Bifurcation, Chaos, Subsynchronous Resonance, Damper Windings, PSS.

1. Introduction:

In power systems series compensation is considered as a powerful technique based on economic and technical considerations for increasing effectively the power transfer capability as well as improving the stability of these systems. However, this introduces problems as well as with the benefits, namely the electromechanical interaction between electrical resonant circuits of the transmission system and the torsional natural frequencies of the turbine-generator rotor. This phenomenon is called subsynchronous resonance (SSR), and it can cause shaft fatigue and possible damage or failure.

The phenomenon of subsynchronous resonance occurs mainly in series capacitor-compensated transmission systems. SSR has been studied extensively since 1970, when a major transmission network in southern California experienced shaft failure to its turbine-generator unit with series compensation. The subsynchronous torques on the rotor is a matter of concern because the turbine-generator shaft itself has natural modes of oscillation that are typical of any spring mass system. It happens that the shaft oscillatory modes are at subsynchronous frequencies. Should the induced subsynchronous torques coincide with one of the shaft natural modes of oscillation, the shaft will oscillate at this natural frequency, sometimes with high amplitude.

Three types of SSR can identify the interaction of the system and the generator under the subsynchronous resonance. They have been called torsional interaction effect, induction generator effect, and transient torque effect. In this research, we focus on the torsional interaction effect, which results from the interaction of the electrical subsynchronous mode with the torsional mode. Several methods have been used in SSR study. The most common of these methods are eigenvalue analysis, frequency scanning, and time-domain analysis. The eigenvalue analysis is used in this research. It is a very valuable technique because it provides both the frequencies of oscillation and the damping at each frequency.

Recently, power system dynamics has been studied using the nonlinear dynamics point of view, which utilizes the bifurcation theory. Actually, power systems have rich bifurcation phenomena. Bifurcation is used to indicate a qualitative change in the features of a system, such as the number and types of solution upon a small variation in the parameters of a system. It has been revealed that there are different types of bifurcation in power system models. In general, the power system model can be represented by a system of nonlinear algebraic and ordinary differential equations.

The bifurcation theorem was used by Zhu *et al.* [1] to demonstrate the existence of a Hopf bifurcation in a single machine infinite busbar (SMIB) power system, in which the dynamics of the damper windings and the AVR are neglected. Nayfeh *et al.* [2] applied the bifurcation theory to a practical series capacitor compensated single machine power system, the BOARDMAN turbine-generator system. Harb *et al.* [3] applied a bifurcation analysis together with the method of multiple scales and Floquet theory to the CHOLLA # 4 turbine-generator system. Tomim *et al.* [4] proposed an index that identifies Hopf bifurcation points in power systems susceptible to subsynchronous resonance. Dobson and Barocio [5] analyzed

general perturbations of a weak resonance and found two distinct behaviors, including interactions near strong resonances in which the eigenvalues quickly change direction.

In this paper, we focus on the torsional interaction effect, which results from the interaction of the electrical subsynchronous mode with the torsional mode. The second system of the IEEE second benchmark model is considered. We use bifurcation theory and chaos to investigate the complex dynamics of the considered system. The type of the Hopf bifurcation is determined by numerical integration of the system, with specific amount of initial disturbances, slightly before and after the bifurcation value. On further increase of the compensation factor, the system experiences chaos via torus attractor. Chaos is a bounded steady-state behavior that is not an equilibrium solution or a periodic solution or a quasiperiodic solution [6].

2. System Description

The system considered is the two different machine infinite bus system, shown in Figure 1. The two machines have a common torsional mode connected to a single series compensated transmission line. The model and the parameters are provided in the second system of the IEEE second benchmark model.

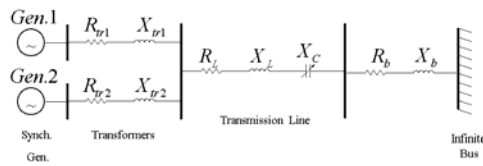


Fig. 1. Electrical system (Two different machine infinite bus system).

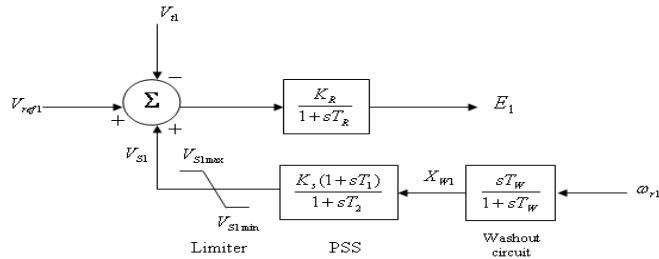


Fig. 3. Block diagram of the use of AVR and PSS to the first generator

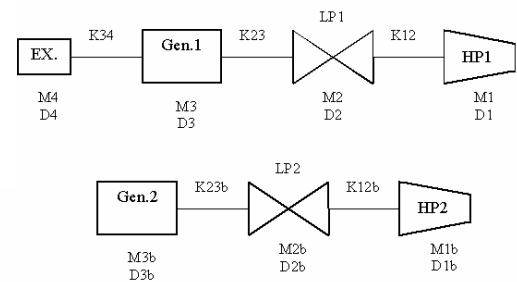


Fig. 2. Electro-mechanical systems for the first and second units.

The electro-mechanical systems for the first and second units are shown in Figure. 2. The first unit consists of exciter (EX.), generator (Gen.1), low-pressure (LP1) and high-pressure (HP1) turbine sections. And the second unit consists of generator (Gen.2), low-pressure (LP2) and high-pressure (HP2) turbine sections. Every section has its own angular momentum constant M and damping coefficient D, and every pair of successive masses have their own shaft stiffness constant K, as shown in Figure 2. The data for electrical and mechanical system are provided in [7]. Replacement of these generators with a single equivalent generator will change the resonance characteristics and therefore is not justified. Consequently, each generator is represented in its own rotor frame of reference and suitable transformation is made.

3. Mathematical Model

The mathematical model of the electrical and mechanical system will be presented in this section. Actually, the electrical system includes the dynamic nonlinear mathematical model of a synchronous generator and that of the transmission line. The generator model considered in this study includes five equations, d-axis stator winding, q- axis stator winding, d-axis rotor field winding, q-axis rotor damper winding and d-axis rotor damper winding equations. Each mass of the mechanical system can be modeled by a second order ordinary differential equation (swing equation), which is presented in state space model as two first order ordinary differential equations.

Using the direct and quadrature d-q axes and Park's transformation, we can write the complete mathematical model that describes the dynamics of the system as follows:

Generator # 1:

$$\begin{aligned}
& - (X_{r1} + X_L + X_b + X_{d1}) \frac{di_{d1}}{dt} - (X_L + X_b) \cos \delta_{r12} \frac{di_{d2}}{dt} - (X_L + X_b) \sin \delta_{r12} \frac{di_{q2}}{dt} \\
& + X_{md1} \frac{di_{f1}}{dt} + X_{md1} \frac{di_{D1}}{dt} = \omega_b \{ (R_{r1} + R_L + R_b + R_{a1}) i_{d1} + [(R_L + R_b) \cos \delta_{r12} \\
& + \left(\frac{\omega_{r2}}{\omega_b} + 1 \right) (X_L + X_b) \sin \delta_{r12}] i_{d2} - \left[\frac{\omega_{r1}}{\omega_b} (X_{r1} + X_L + X_b) + (X_L + X_b) + \omega_{r1} X_{q1} \right] i_{q1} \\
& + \left[(R_L + R_b) \sin \delta_{r12} - \left(\frac{\omega_{r2}}{\omega_b} + 1 \right) (X_L + X_b) \cos \delta_{r12} \right] i_{q2} + X_{mq1} \omega_{r1} i_{Q1} \\
& + e_{cd} \sin \delta_{r1} - e_{cq} \cos \delta_{r1} + V_{0D} \sin \delta_{r1} - V_{0Q} \cos \delta_{r1} \} \tag{1}
\end{aligned}$$

$$\begin{aligned}
& - (X_{r1} + X_L + X_b + X_{q1}) \frac{di_{q1}}{dt} - (X_L + X_b) \cos \delta_{r12} \frac{di_{q2}}{dt} + (X_L + X_b) \sin \delta_{r12} \frac{di_{d2}}{dt} \\
& + X_{mq1} \frac{di_{Q1}}{dt} = \omega_b \{ (R_{r1} + R_L + R_b + R_{a1}) i_{q1} + [(R_L + R_b) \cos \delta_{r12} \\
& + \left(\frac{\omega_{r2}}{\omega_b} + 1 \right) (X_L + X_b) \sin \delta_{r12}] i_{q2} + \left[\frac{\omega_{r1}}{\omega_b} (X_{r1} + X_L + X_b) + (X_L + X_b) + \omega_{r1} X_{d1} \right] i_{d1} \\
& + \left[- (R_L + R_b) \sin \delta_{r12} + \left(\frac{\omega_{r2}}{\omega_b} + 1 \right) (X_L + X_b) \cos \delta_{r12} \right] i_{d2} - X_{md1} \omega_{r1} i_{f1} \\
& - X_{md1} \omega_{r1} i_{D1} + e_{cd} \cos \delta_{r1} + e_{cq} \sin \delta_{r1} + V_{0D} \cos \delta_{r1} + V_{0Q} \sin \delta_{r1} \} \tag{2}
\end{aligned}$$

$$- X_{md1} \frac{di_{d1}}{dt} + X_{f1} \frac{di_{f1}}{dt} + X_{md1} \frac{di_{D1}}{dt} = \omega_b \left[- R_{f1} i_{f1} + \frac{R_{f1} E_{fd1}}{X_{md1}} \right] \tag{3}$$

$$- X_{mq1} \frac{di_{q1}}{dt} + X_{Q1} \frac{di_{Q1}}{dt} = - \omega_b R_{Q1} i_{Q1} \tag{4}$$

$$- X_{md1} \frac{di_{d1}}{dt} + X_{md1} \frac{di_{f1}}{dt} + X_{D1} \frac{di_{D1}}{dt} = - \omega_b R_{D1} i_{D1} \tag{5}$$

where : $v_{f1} = \frac{R_{f1} E_{fd1}}{X_{md1}}$
 $i, j = 1, 2$ and $i \neq j$, $\sin \delta_{rij} = \sin (\delta_{ri} - \delta_{rj})$, $\cos \delta_{rij} = \cos (\delta_{ri} - \delta_{rj})$

Similarly, for the second generator the generator model includes five equations as follows:

$$\begin{aligned}
& - (X_{r2} + X_L + X_b + X_{d2}) \frac{di_{d2}}{dt} - (X_L + X_b) \cos \delta_{r21} \frac{di_{d1}}{dt} - (X_L + X_b) \sin \delta_{r21} \frac{di_{q1}}{dt} \\
& + X_{md2} \frac{di_{f2}}{dt} + X_{md2} \frac{di_{D2}}{dt} = \omega_b \{ (R_{r2} + R_L + R_b + R_{a2}) i_{d2} + [(R_L + R_b) \cos \delta_{r21} \\
& + \left(\frac{\omega_{r1}}{\omega_b} + 1 \right) (X_L + X_b) \sin \delta_{r21}] i_{d1} - \left[\frac{\omega_{r2}}{\omega_b} (X_{r2} + X_L + X_b) + (X_L + X_b) + \omega_{r2} X_{q2} \right] i_{q2} \\
& + \left[(R_L + R_b) \sin \delta_{r21} - \left(\frac{\omega_{r1}}{\omega_b} + 1 \right) (X_L + X_b) \cos \delta_{r21} \right] i_{q1} + X_{mq2} \omega_{r2} i_{Q2} \\
& + e_{cd} \sin \delta_{r2} - e_{cq} \cos \delta_{r2} + V_{0D} \sin \delta_{r2} - V_{0Q} \cos \delta_{r2} \} \tag{6}
\end{aligned}$$

$$\begin{aligned}
& - (X_{r2} + X_L + X_b + X_{q2}) \frac{di_{q2}}{dt} - (X_L + X_b) \cos \delta_{r21} \frac{di_{q1}}{dt} + (X_L + X_b) \sin \delta_{r21} \frac{di_{d1}}{dt} \\
& + X_{mq2} \frac{di_{Q2}}{dt} = \omega_b \{ (R_{r2} + R_L + R_b + R_{a2}) i_{q2} + [(R_L + R_b) \cos \delta_{r21} \\
& + \left(\frac{\omega_{r1}}{\omega_b} + 1 \right) (X_L + X_b) \sin \delta_{r21}] i_{q1} + \left[\frac{\omega_{r2}}{\omega_b} (X_{r2} + X_L + X_b) + (X_L + X_b) + \omega_{r2} X_{d2} \right] i_{d2} \\
& + \left[- (R_L + R_b) \sin \delta_{r21} + \left(\frac{\omega_{r1}}{\omega_b} + 1 \right) (X_L + X_b) \cos \delta_{r21} \right] i_{d1} - X_{md2} \omega_{r2} i_{f2} \\
& - X_{md2} \omega_{r2} i_{D2} + e_{cd} \cos \delta_{r2} + e_{cq} \sin \delta_{r2} + V_{0D} \cos \delta_{r2} + V_{0Q} \sin \delta_{r2} \} \tag{7}
\end{aligned}$$

$$- X_{md2} \frac{di_{d2}}{dt} + X_{f2} \frac{di_{f2}}{dt} + X_{md2} \frac{di_{D2}}{dt} = \omega_b \left[- R_{f2} i_{f2} + \frac{R_{f2} E_2}{X_{md2}} \right] \tag{8}$$

$$- X_{mq2} \frac{di_{q2}}{dt} + X_{Q2} \frac{di_{Q2}}{dt} = - \omega_b R_{Q2} i_{Q2} \tag{9}$$

$$- X_{md2} \frac{di_{d2}}{dt} + X_{md2} \frac{di_{f2}}{dt} + X_{D2} \frac{di_{D2}}{dt} = - \omega_b R_{D2} i_{D2} \tag{10}$$

where : $v_{f2} = \frac{R_{f2} E_2}{X_{md2}}$

Voltage drop across X_c :

$$\frac{de_{cd}}{dt} = \omega_b [X_c I_{LD} + e_{cq}] \quad (11)$$

$$\frac{de_{cq}}{dt} = \omega_b [X_c I_{LQ} - e_{cd}] \quad (12)$$

$$\text{where } \begin{cases} I_{LD} = I_{q1} \cos \delta_1 + I_{q2} \cos \delta_2 + I_{d1} \sin \delta_1 + I_{d2} \sin \delta_2 \\ I_{LQ} = I_{q1} \sin \delta_1 + I_{q2} \sin \delta_2 - I_{d1} \cos \delta_1 - I_{d2} \cos \delta_2 \end{cases}$$

Mechanical System:

High-pressure turbine # 1:

$$\frac{d\omega_1}{dt} = \frac{1}{M_1} [-D_1(\omega_1 - 1) - K_{12}(\theta_1 - \theta_2)] \quad (13)$$

$$\frac{d\theta_1}{dt} = \omega_b(\omega_1 - 1) \quad (14)$$

Low-pressure turbine # 1:

$$\frac{d\omega_2}{dt} = \frac{1}{M_2} [-D_2(\omega_2 - 1) + K_{12}(\theta_1 - \theta_2) - K_{23}(\theta_2 - \delta_{r1})] \quad (15)$$

$$\frac{d\theta_2}{dt} = \omega_b(\omega_2 - 1) \quad (16)$$

Similarly, for the second High- and low-pressure turbine:

High-pressure turbine # 2:

$$\frac{d\omega_{1b}}{dt} = \frac{1}{M_{1b}} [-D_{1b}(\omega_{1b} - 1) - K_{12b}(\theta_{1b} - \theta_{2b})] \quad (17)$$

$$\frac{d\theta_{1b}}{dt} = \omega_b(\omega_{1b} - 1) \quad (18)$$

Low-pressure turbine # 2:

$$\frac{d\omega_{2b}}{dt} = \frac{1}{M_{2b}} [-D_{2b}(\omega_{2b} - 1) + K_{12b}(\theta_{1b} - \theta_{2b}) - K_{23b}(\theta_{2b} - \delta_{r2})] \quad (19)$$

$$\frac{d\theta_{2b}}{dt} = \omega_b(\omega_{2b} - 1) \quad (20)$$

Generator # 1:

$$\frac{d\omega_{r1}}{dt} = \frac{1}{M_3} [T_{m1} - T_{e1} + K_{23}(\theta_2 - \delta_{r1}) - K_{34}(\delta_{r1} - \theta_4) - D_3(\omega_{r1} - 1)] \quad (21)$$

$$\frac{d\delta_{r1}}{dt} = \omega_b(\omega_r - 1) \quad (22)$$

$$\text{where } \begin{cases} T_{e1} = i_{q1}\Psi_{d1} - i_{d1}\Psi_{q1} \\ = (X_{q1} - X_{d1})i_{d1}i_{q1} + X_{md1}i_{f1}i_{q1} - X_{mq1}i_{Q1}i_{d1} + X_{md1}i_{D1}i_{q1} \end{cases}$$

Generator # 2:

$$\frac{d\omega_{r2}}{dt} = \frac{1}{M_{3b}} [T_{m2} - T_{e2} + K_{23b}(\theta_{2b} - \delta_{r2}) - D_{3b}(\omega_{r2} - 1)] \quad (23)$$

$$\frac{d\delta_{r2}}{dt} = \omega_b(\omega_{r2} - 1) \quad (24)$$

$$\text{where } \begin{cases} T_{e2} = i_{q2}\Psi_{d2} - i_{d2}\Psi_{q2} \\ = (X_{q2} - X_{d2})i_{d2}i_{q2} + X_{md2}i_{f2}i_{q2} - X_{mq2}i_{Q2}i_{d2} + X_{md2}i_{D2}i_{q2} \end{cases}$$

Exciter:

$$\frac{d\omega_4}{dt} = \frac{1}{M_4} [-D_4(\omega_4 - 1) + K_{34}(\delta_{r1} - \theta_4)] \quad (25)$$

$$\frac{d\theta_4}{dt} = \omega_b(\omega_4 - 1) \quad (26)$$

The mathematical models of AVR and PSS (shown in Figure 3) can be written as follows:

$$\frac{d\omega_{r1}}{dt} - \frac{dX_{w1}}{dt} = \frac{1}{T_w} X_{w1} \quad (27)$$

$$K_s T_1 \frac{dX_{w1}}{dt} - T_2 \frac{dV_{s1}}{dt} = V_{s1} - K_s X_{w1} \quad (28)$$

$$T_R \frac{dE_{t1}}{dt} = K_R (V_{ref1} + V_{s1} - V_{t1}) - E_{t1} \quad (29)$$

Where: $V_{t1} = \sqrt{V_{d1}^2 + V_{q1}^2}$

Neglecting stator transients yields:

$$V_{d1} = -R_{a1} i_{d1} + X_{q1} i_{q1}$$

$$V_{q1} = -R_{a1} i_{q1} - X_{d1} i_{d1} + X_{md1} i_{fd1}$$

Consequently,
$$V_{t1} = \sqrt{(-R_{a1} i_{d1} + X_{q1} i_{q1})^2 + (-R_{a1} i_{q1} - X_{d1} i_{d1} + X_{md1} i_{fd1})^2} \quad (30)$$

Therefore, these systems can be mathematically modeled as a set of first order nonlinear ordinary differential equations with the compensation factor ($\mu = X_c/X_l$) as a bifurcation (control) parameter. So, bifurcation theory can be applied to nonlinear dynamical systems, which can be written in the form $dx/dt=F(x;\mu)$.

4. System Response Without Damper Windings, AVR and PSS

To study the case of neglecting the dynamics of d- and q-axes damper windings, we set $i_{D1}=i_{Q1}=0$ and $i_{D2}=i_{Q2}=0$ in (4, 5, 9 and 10). Then, the dynamics of the system are governed by (1-3, 6-8, and 11-26). At any value of the compensation factor μ , the operating points (equilibrium solutions) are obtained by setting the derivatives of the 22 state variables in the system equal to zero. The stability of the equilibrium solution is studied by examination of the eigenvalues of the Jacobian matrix evaluated at the operating point. There are 20 complex conjugate eigenvalues and two real eigenvalues. The operating point stability regions are shown in Figure 4. It can be observed that the power system has stable operating point in the region $0 < \mu < H \approx 0.420692$, unstable operating point in the region $H \approx 0.420692 < \mu \leq 1$ and a Hopf bifurcation point at $\mu = H \approx 0.420692$.

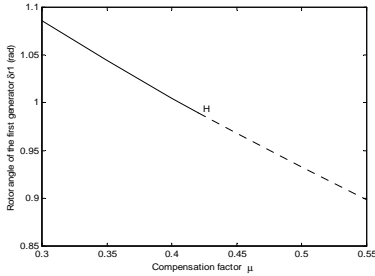


Fig. 4. Bifurcation diagram showing variation of the first generator rotor angle δ_{r1} with the compensation factor μ .

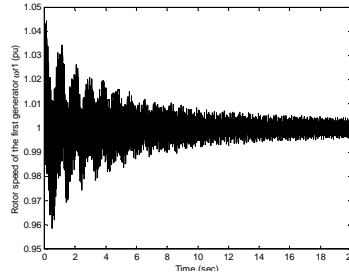


Fig. 5. Rotor speed of the first generator at $\mu=0.410600$ with 5% initial disturbance in rotor speed of generator.

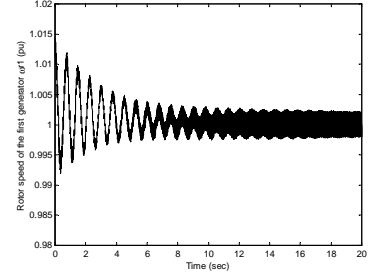


Fig. 6. Rotor speed of the first generator at $\mu=0.420760$ with 2% initial disturbance in rotor speed of generator.

Figure 5 shows the response of the system with 5% initial disturbance on the speed of the generator at $\mu=0.410600$, which is less than H . It can be observed that, the system is stable. While Figure 6 shows the system response after a 2% initial disturbance in generator rotor speed at $\mu=0.420760$, which is greater than H . It can be observed that, the system routes to a periodic solution giving rise to oscillations. Hence, the type of this Hopf bifurcation is supercritical. So, the periodic solution emanating at the bifurcation point is stable.

Figure 7 shows the two-dimensional projections and time histories of the system at different compensation factors. It can be observed that, at $\mu=0.420692$ the system oscillates just at one frequency with a small amplitude limit cycle. While it oscillates with more than one incommensurate frequency slightly after the bifurcation point at $\mu=0.421583$ and obtain a period quasiperiodic attractor. As the compensation factors increase further, up to $\mu=0.423580$, the system oscillates at infinite number of incommensurate frequencies. The motion is still bounded. This is however called chaos.

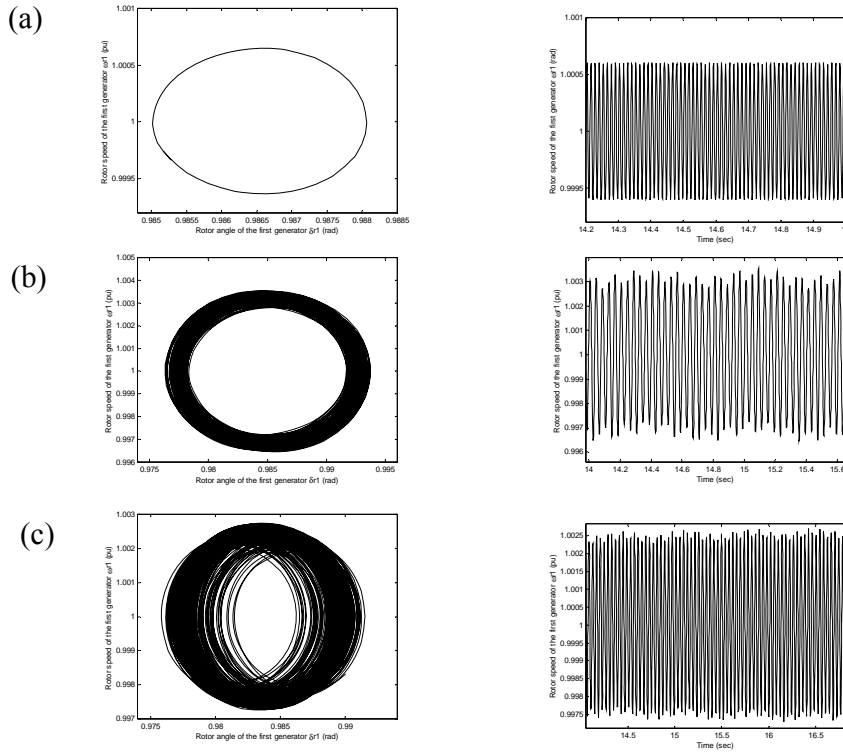


Fig. 7. Two-dimensional projection of the phases portrait onto $\omega_m - \delta_m$ plane (left) and the time histories of the corresponding rotor speed of generator (right). The solution at (a) limit cycle ($\mu = 0.420692$), (b) torus-attractor ($\mu = 0.421583$), and (c) chaotic attractor ($\mu = 0.423580$). (For the case of no damper windings).

5. Addition of Damper Windings

In this section, we study the effect of adding damper windings on both axes of the first generator. We evaluate the influence of these damper windings on the Hopf bifurcations. Although damper windings have some benefits in transient stability, such as damping off speed oscillations, they may induce subsynchronous resonance [8]. We will show that damper windings reduce the compensation level at which subsynchronous resonance occurs.

In this case we have 24 ordinary nonlinear differential equations, (1-8, 11-26). As in the previous section, the stability of the equilibrium solution is studied by examination of the eigenvalues of the Jacobian matrix evaluated at the operating point. There are 22 complex conjugate eigenvalues and four real eigenvalues.

The operating point stability regions in the $\delta_{r1}-\mu$ plane together with two Hopf bifurcation points are depicted in Figure 8.

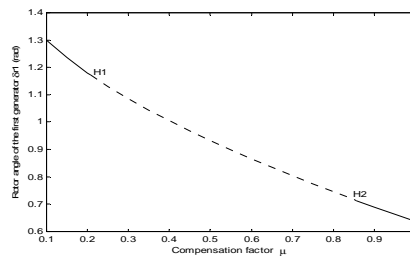


Fig. 8. Bifurcation diagram showing variation of the first generator rotor angle δ_{r1} with the compensation factor μ , (For the case of adding both damper windings to the first generator).

We observe that the power system has a stable operating point to the left of $H_1 \approx 0.207621$ and to the right of $H_2 \approx 0.857447$, and has an unstable operating point between H_1 and H_2 . The operating point loses stability at a Hopf bifurcation point where $\mu = H_1$, the type of this Hopf bifurcation is supercritical. While it regains stability at a reverse Hopf bifurcation for $\mu = H_2$. In this case a pair of complex conjugate eigenvalues will transversally cross from left half and right half of the complex plane, and then back to left half. According to the Hopf bifurcation theory, a Hopf bifurcation of a fixed point of a continuous-time system leads to a periodic solution. So, a limit cycle is born at $\mu = H_1 \approx 0.206721$.

6. Addition of Damper Windings, AVR and PSS

In this section we investigate the influence of adding damper windings, automatic voltage regulator (AVR) and power system stabilizer (PSS) to the first generator. The automatic voltage regulator (AVR) controls the excitation voltage of the synchronous generator with the terminal voltage of synchronous generator as an input signal, while the output signal is the d-axis field voltage. Power system stabilizer (PSS) uses auxiliary (supplementary) stabilizing signals to control the excitation system so as to improve power system dynamic performance. Commonly used input signals to PSS are shaft speed, terminal frequency or power. Power system dynamic performance can be improved by the damping of system oscillations. This is a very effective method of enhancing small-signal stability performance. In this study, the input signal to the PSS is the generator rotor speed. Figure 3 shows the block diagram of the use of AVR together with the PSS [9]. The first block on the right side that is used to wash out the compensation effect after a time lag T_W , with a typical values between 4 to 20 sec.

In this study, the mathematical model of the system is extended to 27 differential equations by including (27)-(30). The internal generated voltage E_1 of the first synchronous generator is no more a fixed value i.e. E_1 in addition to X_{W1} and V_{S1} are the new state variables. The output of the PSS is one of the inputs of the AVR. The other inputs are V_{ref1} and the terminal voltage of the synchronous generator V_{t1} . The terminal voltage is not a state variable, but it can be expressed in terms of other state variables, (30). As in the previous cases, the stability of the equilibrium solution is studied by examination of the eigenvalues of the Jacobian matrix evaluated at the operating point. This study is carried out on a heavily loaded synchronous generator with $V_{t1}=1.14$, $V_{ref1}=1.152$ and $T_m=0.91$ pu at a compensation factor $\mu = 0.1$.

In addition to the parameters given before, the parameters for the AVR and PSS are:

$$K_R = 200, T_R = 0.025 \text{ sec.}, T_W = 10 \text{ sec.}, K_S = 12, T_I = 0.048 \text{ sec.}, T_2 = 0.032 \text{ sec.}$$

In this case, a new stable oscillatory mode with a frequency of 3.65 Hz and a stable real eigenvalue were added. The operating point stability regions in the δ_{r1} plane together with two Hopf bifurcation points are depicted in Figure 9.

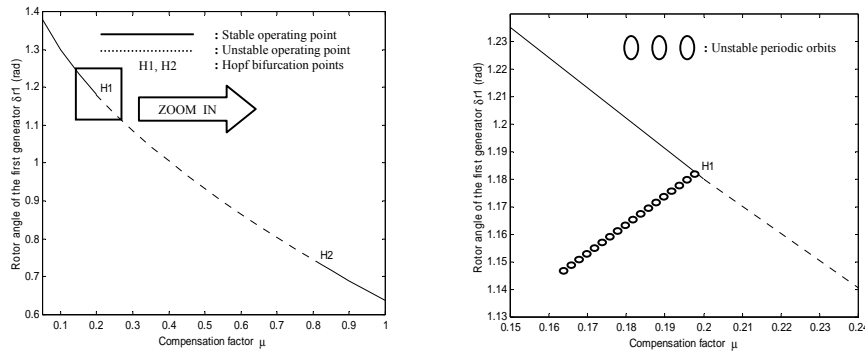


Fig. 9. Bifurcation diagram showing variation of the first generator rotor angle δ_{r1} with the compensation factor μ (for the case of including damper windings, AVR and PSS to the first generator).

We observe that the power system has a stable operating point to the left of $H_1 \approx 0.198377$ and to the right of $H_2 \approx 0.824135$, and has an unstable operating point between H_1 and H_2 . The operating point loses stability at a Hopf bifurcation point, namely $\mu = H_1$. It regains stability at a reverse Hopf bifurcation, namely $\mu = H_2$. In this case a pair of complex conjugate eigenvalues will transversally cross from left half to right half of the complex plane, and then back to the left half.

To determine whether the limit cycles created due to the Hopf bifurcation are stable or unstable, we obtain the time response of the system by numerical integration with small disturbance slightly before H_1 . Figure 10 shows the response of the system with 7% initial disturbance on the speed of the generator at $\mu=0.182265$, which is less than H_1 . It can be observed that the system is unstable. Therefore, the type of this Hopf bifurcation is subcritical. So, the periodic solution emanating at the bifurcation point is unstable.

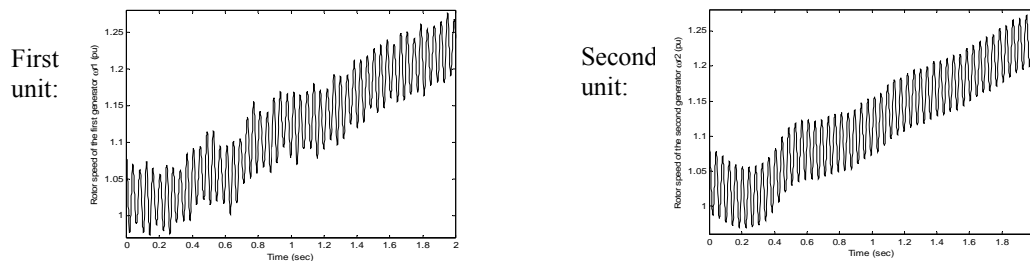


Fig. 10 Rotor speed of the generator at $\mu = 0.199135$ with 7% initial disturbance in rotor speed of generator, (For the case of including damper windings, AVR and PSS to the first generator).

7. Conclusions

Bifurcation theory is applied to the second system of the IEEE second benchmark model of SSR to investigate the complex dynamics of the system. The case of neglecting the dynamics of both damper windings is considered. The results show that as the compensation factor ($\mu = X_c/X_d$) increases the operating point loses stability via **Hopf bifurcation** point. The type of the Hopf bifurcation can be determined by numerical method based on the response of the perturbed system. Also, the influence of adding damper windings along the q- and d-axes on subsynchronous resonance has been investigated. The results show that these damper windings affect the locations, number and type of the Hopf bifurcations. Adding damper windings shift the Hopf bifurcation to smaller value of μ and hence shrink the stable region. In other words, the damper windings **destabilize the system** by reducing the compensation level at which subsynchronous resonance occurs. In the case of adding damper windings, AVR and PSS the Hopf bifurcation slightly shifted to the left. Also, the results showed that the type of this Hopf bifurcation is **subcritical**. Consequently, we can conclude that the change of Hopf bifurcation caused by AVR and PSS is mainly qualitative with some quantitative change.

References

- [1] W. Zhu, R.R. Mohler, R. Spce, W.A. Mittelstadt and D. Maratukulman, "Hopf Bifurcation in a SMIB Power System with SSR," IEEE Trans. on Power Systems, Vol.11, No.3, pp. 1579-1584, 1996.
- [2] A.H Nayfeh, A.M. Harb, and C-M.Chin, A.M. Hamdan and L. Mili, Application of Bifurcation Theory to Subsynchronous Resonance in Power Systems, Int.J.Bifurcation and Chaos, Vol.8, No.1, pp.157-172, 1998
- [3] A. M. Harb, A. H. Nayfeh, and L. Mili, "Bifurcation Control for Mitigating Subsynchronous Oscillations in Power Systems", 14th PSCC, Sevilla, 24-28 June 2002.
- [4] M. A. Tomim, A. C. Zambroni de Souza, P. P. Carvalho Mendes, and G. Lambert-Torres, "Identification of Hopf Bifurcation in Power Systems Susceptible to Subsynchronous Resonance", IEEE Bologna Power Tech Conference, June 23-26, 2003, Bologna, Italy.
- [5] I. Dobson and E. Barocio, "Perturbations of Weakly Resonant Power System Electromechanical Modes", IEEE Bologna Power Tech Conference, June 23-26, 2003, Bologna, Italy.
- [6] A.H. Nayfeh and B. Balachandran, Applied Nonlinear Dynamics, Wiley, New York, 1995.
- [7] IEEE SSR Working Group, "Second Benchmark Model for Computer Simulation of Subsynchronous Resonance," IEEE Trans. On Power Apparatus and Systems. Vol. PAS- 104, No.5, 1057-1064, May 1985.
- [8] A.H Nayfeh, A.M. Harb, and C-M.Chin, A.M. Hamdan and L. Mili, Application of Bifurcation Theory to subsynchronous Resonance in Power Systems, Int.J.Bifurcation and Chaos, Vol.8, No.1, pp.157-172, 1998
- [9] K.R. Padiyar, M.K. Geetha and K.U. Rao, "A Novel Power Flow Controller for Controlled Series Compensation," IEE, AC and DC Power Transmission, 29 April-3 May, Conference Publication No. 423, pp. 329-334, 1996.